Direct signal cancellation in passive bistatic DVB-T based radar

Hilde Kjelgaard Brustad

FFI Forsvarets
forskningsinstitutt

Direct signal cancellation in passive bistatic DVB-T based radar

Hilde Kjelgaard Brustad

Keywords

Radar

Støy

Signalbehandling

Approved by

Karl Erik Olsen   Project Manager

Johnny Bardal   Director

English summary

Passive radars receive target reflections from transmitters of opportunity. They do not emit any radiation, which makes them harder to find. A challenge with the passive radar is to suppress the strong direct signal incoming at the surveillance antenna, emitted from the transmitter, in order to be able to detect weaker targets. A direct signal cancellation method called "Extensive Cancellation Algorithm" is the focus of this report. The algorithm minimizes the contribution of the direct signal to the surveillance signal, by means of a least mean squares method. We demonstrate the use of this cancellation algorithm on real data, and give an estimate on how much the signal to noise ratio of a target can be increased.

Two different antenna configurations are used. Antenna configuration A has an angle of about $90°$ between the direction to the transmitter and the surveillance antenna main lobe. In configuration B, the surveillance antenna is pointing towards the transmitter, which should maximize the direct signal interference.

The target signal to noise ratio of ten targets observed with antenna configuration A experience an average increase of about 10dB after direct signal cancellation. The average increase is about 20dB for configuration B. Some targets from this configuration had initially a signal level lower than the estimated noise floor. After cancellation, the SNR had increased such that they were able to be detected as a target. The corresponding reduction in noise floor level are about 10dB and 14dB for configuration A and B, respectively. The result show that the effect of direct signal cancellation depends on where the direct signal interferes in the surveillance antennas antenna pattern.

Sammendrag

Passive radarsystemer benytter seg av signaler sendt ut fra f.eks. kringkastingssendere. De trenger derfor ikke sende ut stråling, noe som gjør de vanskelige å oppdage. En utfordring med et passivt radarsystem er å undertrykke det sterke direktesignalet fra senderen som kommer inn i overvåkingsantennen, for å gjøre det mulig å oppdage svakere mål. Fokuset i denne rapporten vil være en metode for undertrykking av direktesignalet kalt "Extensive Cancellation Algorithm". Metoden minimerer bidraget fra direktesignalet i overvåkingssignalet ved hjelp av minste kvadraters metode. Denne metoden for kansellering blir vist på reelle data, og det gis et estimat på hvor mye signal til støy forholdet på mål kan økes ved hjelp av kansellering.

To forskjellige antennekonfigurasjoner er benyttet for opptak av data. For antennekonfigurasjon A er vinkelen mellom overvåkingsantennens hovedlobe og sendenren på omtrent $90°$. For konfiguration B peker overvåkingsantennens hovedlobe mot senderen.

Den gjennomsnittlige økningen i signal til støy forhold for ti mål observert med antennekonfigurasjon A er på rundt 10dB. Den gjennomsnittlige økningen er på omtrent 20dB for konfigurasjon B. Enkelte mål fra konfigurasjon B hadde før kansellering et signal som lå lavere enn det estimerte støygulvet. Etter kansellering hadde signalet økt til et nivå som kan detekteres som et mål. Reduksjonen i det estimerte støygulvet er på henholdsvis 10dB og 14dB for konfigurasjon A og B. Resultatene viser at effekten av kansellering er avhengig av hvor i overvåkingantennens antennemønster direktesignalet forstyrrer.

Contents

1 Introduction

Passive radars have the advantage that they are almost invisible in the electromagnetic scene, in the sense that they do not emit any signals. Passive radars exploit signals from transmitters of opportunity, such as FM, DAB and DVB-T signals.

A typical antenna configuration for a passive bistatic radar consists of a reference antenna and a surveillance antenna. The reference antenna is directed towards a transmitter and intercept the emitted signal. A surveillance antenna then looks for targets, from which the transmitted signal has been reflected. The surveillance signal and reference signal are then compared in order to identify bistatic range and Doppler frequencies of the targets.

A problem with the passive radar can be that the strong direct signal at zero Doppler emitted from the transmitter is also received by the surveillance antenna. Because of the sidelobes in the ambiguity function of the emitted waveform, the direct signal interference can cause weaker targets at nonzero Doppler frequencies, and at any bistatic range, to vanish into the background of noise.

One possible countermeasure, is to physically place a shield in the direction of the transmitter. This is not always possible, and there may be contributions of the direct signal from other incoming angles, caused by reflections from, e.g., nearby buildings and terrain. By exploiting a narrow beam antenna, the direct signal interference can be suppressed in the sidelobes of the antenna pattern. On the other hand, such an antenna is not suitable as a fixed surveillance antenna, where a wider beam is prefered. If the surveillance antenna is a phased array antenna, the antenna pattern could be modified such that a notch in the antenna pattern is placed in the direction of the transmitter.

An alternative to the above methods of cancellation is to suppress the direct signal (and its time delayed copies) by means of a direct signal cancellation (DSC) algorithm implemented in digital signal processing. This report is going elaborate a DSC algorithm called Extensive Cancellation Algorithm, derived by means of the least mean squares method [1, 2]. The aim of the work is to demonstrate the use of DSC on real data and how much the target signal to noise ratio can be increased.

DSC is not only limited to suppressing direct signal interference, but can also be used in a modern active radar to suppress signals from e.g. a jammer or strong signals from targets that masks other weaker targets [3].

The data processed in this report are recorded with a passive radar system that exploits DVB-T signals to detect and track aircraft and other targets of interest. The Norwegian DVB-T signals are located between 470MHz and 790MHz, partitioned into channels of 8MHz [4]. Data processed in this report are recorded from channels with center frequency 546MHz and 722MHz. For data recorded in the lower frequency band, both the reference antenna and the surveillance antenna are directed towards the transmitter. At the higher frequency, the angle between the surveillance antenna main lobe and the direction to the transmitter is about $90°$. This difference in orientation of the surveillance antennas of

the configurations, makes the direct signal interfere at different angles in the antenna pattern of the surveillance antennas, which will affect the result of direct signal cancellation.

Section 2 explains the processing of the recorded data before cancellations begin. The section shows the I/Q demodulation and down sampling of the digitized data and how range Doppler (RD) processing is performed. In section 3.2 a noise analysis are performed, and a signal to noise ratio (SNR) gets defines. The Extensive Cancellation Algorithm for signal cancellation is presented in section 4. Measurement setup, parameters used and results from cancellation applied on recorded data are presented in section 5. Discussion of the results regarding DSC are given in section 6.

2   Signal processing prior to cancellation

2.1   Analog-to-digital conversion

In this report, we use data recorded from the 8MHz DVB-T bands with center frequency 546MHz and 722MHz. The center frequency of the signal is through several stages mixed down to 76MHz and real sampled with a sampling rate $f_s = 64$MHz. This results in an undersampling of the signal. The DVB-T channel of interest is then located between 8Hz and 16MHz [5]. The sampled real data from the reference and surveillance antenna are then stored as 16-bit signed integers. The data processed further are later scaled to lie in the range $[-1, 1]$. The left panel of figure 2.1 show the frequency spectrum of the real sampled data.

2.2   I/Q demodulation and down sampling

In order to easily extract and modify phase information of the recorded data, and to be able to down sample the signal, and reduce the amount of data, the data needs to be I/Q demodulated and shifted in frequency. First, we apply a band pass filter in order to eliminate any frequencies outside of the 8MHz band of interest. A rectangular filter with amplitude 1 in the range $[8\text{MHz}, 16\text{MHz}]$ and zero elsewhere is used. The band pass filter removes "negative frequencies" of the real signal (whose Fourier-components are the complex conjugate of the positive frequency components), and the result is a complex signal. The frequency band of interest is shifted down to lie between -4MHz and 4MHz and, by the Nyquist criterion, the signal can be resampled at 8MHz. The amount of data is reduced by a factor of 4. The right panel of figure 2.1 shows the frequency spectrum of the I/Q demodulated signal.

2.3   Range-Doppler processing

After the reference signal ($\boldsymbol{s}_{ref}$) and one surveillance signal ($\boldsymbol{s}_{sur}$) have been I/Q demodulated and down sampled, range-Doppler processing (RD processing) can begin. The intention of the RD processing is to identify the bistatic range and bistatic Doppler frequencies of targets. The processing is based on the cross correlation between the reference signal and the surveillance signal for Doppler frequencies of interest, given by
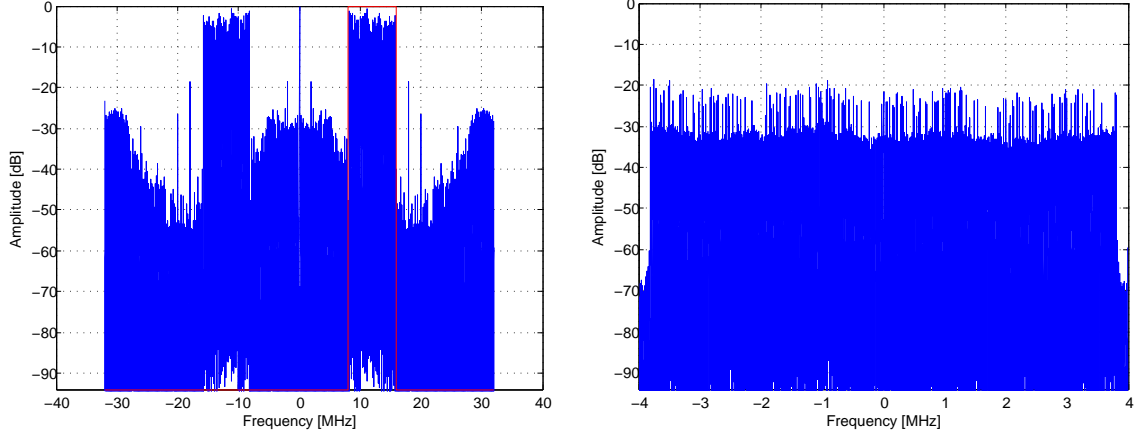
Figure 2.1   Left figure: Frequency spectrum of real sampled signal. The red line shows the rect-angular band pass filter applied. Right figure: Frequency spectrum of signal after I/Q demodulation and down sampling. The DVB-T band of interest has center frequency 722 MHz.

$$c[n, f_D] = \sum_{k=0}^{T-1} \boldsymbol{s}_{ref}^*[k] \boldsymbol{s}_{sur}[k+n] e^{-j2\pi f_D \frac{k}{f_s}} \tag{2.1}$$

where $j = \sqrt{-1}$, f_D is the Doppler frequency of interest and n denotes the time delay in samples. T denotes the number of samples of the surveillance and reference signal (hence the integration time). By increasing the integration time, more energy reflected from a target is present in the signal. On the other hand, if the integration time becomes too long, unwanted range walk and Doppler walk occur, which limit the target signal to noise ratio that can be achieved with coherent integration. Range and Doppler walk are not going to be reviewed in this report. Detailed information on the subject can be found in [6].

(2.1) can be evaluated in several different ways, as described in [7]. The approach used in this report is explained in [7] on page 301-303. This is an effective method for evaluating (2.1) for many ranges and many different Doppler frequencies at the same time. First consider the index k. Redefine this index as

$$k = i + sN \,, \quad i = 0, 1, 2, \ldots, N-1 \,, \quad s = 0, 1, 2, \ldots, M-1 \tag{2.2}$$

such that $NM - 1 \leq T$. i can bee seen as the summing index across the fast time, while s is the summing index across the slow time. (2.1) can now be written as

$$
\begin{aligned}
c[n, f_D] &= \sum_{s=0}^{M-1} \sum_{i=0}^{N-1} \boldsymbol{s}_{ref}^*[i+sN] \boldsymbol{s}_{sur}[i+sN+n] e^{-j2\pi f_D \frac{i+sN}{f_s}} \\
&= \sum_{s=0}^{M-1} e^{-j2\pi f_D \frac{sN}{f_s}} \sum_{i=0}^{N-1} \boldsymbol{s}_{ref}^*[i+sN] \boldsymbol{s}_{sur}[i+sN+n] e^{-j2\pi f_D \frac{i}{f_s}}.
\end{aligned}
\tag{2.3}
$$

With N and f_D sufficiently small such that

$$\frac{f_D N}{f_s} \ll 1 \tag{2.4}$$

the last sum of (2.3) becomes the correlation

$$R[n,s] = \sum_{i=0}^{N-1} \boldsymbol{s}^*_{ref}[i+sN]\boldsymbol{s}_{sur}[i+sN+n] \tag{2.5}$$

between the surveillance signal and the reference signal. Choosing the Doppler frequencies as

$$f_{D,m} = \frac{m f_s}{NM}, \tag{2.6}$$

(2.3) can be recognized as the discrete Fourier transform (DFT) [8]

$$RD[n,m] \sum_{s=0}^{M-1} R[n,s] e^{-j2\pi f_{D,m} s \frac{N}{f_s}} \tag{2.7}$$

There is a disadvantage with this method for range Doppler processing [7]. Because of the assumption made in (2.4), Doppler shifts between the selected portion of the reference and surveillance signal is not compensated for during the correlation in (2.5), and there will be a degradation of the correlation. The larger the Doppler shifts are, the greater the degradation is. $m = \pm M/2$ (given by the implementeation of (2.5) in section 2.3.2) gives the highest value of f_D, such that $f_s N/f_s = 1/2$. A degradation are therefore going to occur for large values of f_D, but the degradation is small, such that the method for RD processing still can be used.

The above method for RD processing therefore mainly consists of three steps: Stacking of data matrices (section 2.3.1), cross correlation between the reference signal and the surveillance signal (section 2.3.2), and then extracting the Doppler frequencies (section 2.3.3).

2.3.1 Stacking data matrices

By redefining the index of the signals as in (2.2), matrices for the reference signal and the surveillance signals can be made. The total number of samples from the reference signal needed in order to construct the reference matrix S_{ref} given as

$$S_{ref} = \begin{bmatrix} s_{ref}[0] & s_{ref}[N] & \cdots & s_{ref}[(M-1)N] \\ s_{ref}[1] & s_{ref}[N+1] & \cdots & s_{ref}[(M-1)N+1] \\ \vdots & \vdots & \ddots & \vdots \\ s_{ref}[N-1] & s_{ref}[2N-1] & \cdots & s_{ref}[MN-1] \\ 0 & 0 & \cdots & 0 \\ 0 & 0 & \cdots & 0 \\ \vdots & \vdots & \ddots & \vdots \\ 0 & 0 & \cdots & 0 \end{bmatrix} \tag{2.8}$$

is then NM. S_{ref} has been zero-padded at the end in order to compensate for the cyclic arrays that a fast Fourier transform (FFT), used to implement the correlation in (2.5), assumes. When the number of samples N has been decided, which gives the maximum range of the processing, the number of columns used to construct the matrix is decided by the integration time T_{CPI}, which are given by

$$T_{CPI} = \frac{NM}{fs}.$$

The final dimension of the reference matrix then becomes $2N \times M$.

The surveillance matrix S_{sur} has the same dimensions as the reference matrix, but because this matrix is not zero-padded, a total amount of $(M+1)N$ samples are needed from the surveillance signal. The matrix is constructed as

$$S_{sur} = \begin{bmatrix} s_{sur}[0] & s_{sur}[N] & \cdots & s_{sur}[(M-1)N] \\ s_{sur}[1] & s_{sur}[N+1] & \cdots & s_{sur}[(M-1)N+1] \\ \vdots & \vdots & \ddots & \vdots \\ s_{sur}[2N-1] & s_{sur}[3N-1] & \cdots & s_{sur}[(M+1)N-1] \end{bmatrix}. \tag{2.9}$$

2.3.2 Cross correlation

The next step is then to perform a cross correlation between the reference matrix and the surveillance matrix. A correlation as given in (2.5) is a time consuming operation that requires many calculations. A new vector s_{sur} has to be made for each delay n, and the sum has to be performed for each delay as well. However, (2.5) can be carried out in the frequency domain by exploiting the correlation theorem [8]. By implementing the Fourier transforms using the fast Fourier transform algorithm, the number of calculations are reduced from N^2 to $N \log N$. In order for the FFT to be as fast as possible, the dimensions of the reference and surveillance matrices in range should be such that $N = 2^l$ for any positive integer l. The result of the cross correlation between the reference matrix and the surveillance matrix is then the range matrix R expressed as

$$R[n,s] = \mathcal{F}^{-1}\big(\mathcal{F}^*(S_{ref})\mathcal{F}(S_{sur})\big) \tag{2.10}$$

where the Fourier transforms have been taken along each column. Each row in the range matrix R represents the time delay between the reference signal and the surveillance signal, which can be translated into bistatic range. The lower half of R can be removed (because of the zero padding), such that the R has N rows and M columns. The maximum processing bistatic range r_{max} and the range bin size Δr then become

$$r_{max} = c\frac{N}{f_s} \quad , \qquad \Delta r = \frac{c}{f_s} \tag{2.11}$$

where c denotes the speed of light in vacuum. The maximum range is dependent on the dimension N, and the bin size is given by the sampling frequency.

2.3.3 Doppler frequencies

After the correlation between the surveillance and reference matrices have been performed, the DFT (2.7) along each row of the matrix $R[n, m]$ can be done. For faster calculations, the DFT is implemented using the FFT, where the number of columns should be such that $M = 2^k$, for any integer k. The result is now a RD matrix, $RD[n, m]$, where each row n represents a specific range, and each column m a specific Doppler shift. Figure 2.2 shows the RD matrix as a grid in range and Doppler, where the value of each component in the matrix is the response of the surrounding scene for that specific range and Doppler.

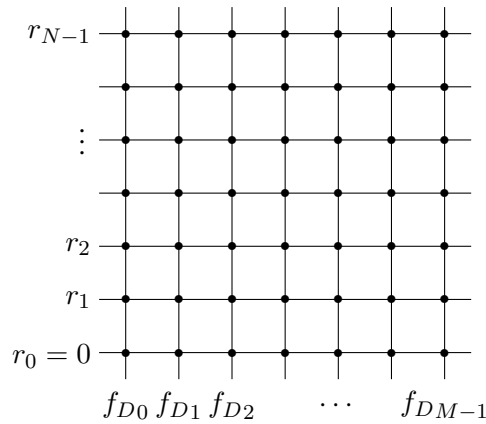*Figure 2.2   Schematic overview of the RD matrix.*

The upper limit for the Doppler frequency is dependent on the sampling frequency and the dimension N. Doppler frequencies lie in the range

$$-\frac{f_s}{2N} \le f_D \le \frac{f_s}{2N} - \frac{f_s}{NM}.$$

The possible Doppler frequencies are decided by the DFT algorithm, as given in (2.6), and the final range of frequencies by the FFT algorithm.

Increasing the dimension M in Doppler does not affect the upper limit for the maximum Doppler frequencies, but rather determines the size of each Doppler bin, which is given as

$$\Delta f_D = \frac{f_s}{NM}.$$

3 Noise analysis

3.1 Noise sample probability distribution

The upper panels of figure 3.1 show histograms of the real part of 50601 noise samples from RD processed data before and after cancellation. From this we can assume that the noise of the system is white Gaussian noise [9, 10]. For sampled I/Q demodulated data, this means that one $\boldsymbol{I}$ (the real part of the noise samples) sample is independent of any other $\boldsymbol{I}$ sample at any other time, and that the $\boldsymbol{I}$ samples have a normal probability distribution function with zero mean, and standard deviation σ given by

$$p(\boldsymbol{I}) \quad = \quad \frac{1}{\sigma\sqrt{2\pi}}e^{-\frac{\boldsymbol{I}^2}{2\sigma^2}}. \tag{3.1}$$

The imaginary part of the noise samples, $\boldsymbol{Q}$, is assumed to follow the same probability distribution. With zero mean, the expectancy value of the squared of the real or imaginary part is equal to the standard deviation σ, which is assumed to be the same for both the real and imaginary part of the samples, and can be found by

$$E[\boldsymbol{I}^2] \quad = \quad E[\boldsymbol{Q}^2] \tag{3.2}$$

$$= \quad \sigma^2 \tag{3.3}$$

$$\approx \quad \frac{1}{N-1}\sum_{n=1}^{N}\boldsymbol{I}[n]^2 \tag{3.4}$$

where N is the number of noise samples. The real and imaginary part of the noise samples are independent, random variables, and the two-dimensional joint PDF for the variables, $p(\boldsymbol{I}, \boldsymbol{Q})$ can be expressed as the product between $p(\boldsymbol{I})$ and $p(\boldsymbol{Q})$

$$p(\boldsymbol{I}, \boldsymbol{Q}) = \frac{1}{2\pi\sigma^2}e^{-\frac{\boldsymbol{I}^2+\boldsymbol{Q}^2}{2\sigma^2}},$$

By introducing the amplitude A and phase θ, with the relation to the real and imaginary part as

$$\boldsymbol{A} = \sqrt{\boldsymbol{I}^2 + \boldsymbol{Q}^2} \quad , \qquad \boldsymbol{\theta} = \arctan\frac{\boldsymbol{Q}}{\boldsymbol{I}} \tag{3.5}$$

a change of variables can be made. The PDF for the new variables then become

$$
\begin{aligned}
p(\boldsymbol{A}, \boldsymbol{\theta}) &= \frac{p(\boldsymbol{I}, \boldsymbol{Q})}{|J(\boldsymbol{I}, \boldsymbol{Q})|} \\
&= \frac{\boldsymbol{A}}{2\pi\sigma^2} e^{-\frac{\boldsymbol{A}^2}{2\sigma^2}}
\end{aligned}
$$

where $J(\boldsymbol{I}, \boldsymbol{Q})$, the Jacobian of the transformation, is calculated as

$$
J(\boldsymbol{I}, \boldsymbol{Q}) = \begin{vmatrix} \frac{\partial \boldsymbol{A}}{\partial \boldsymbol{I}} & \frac{\partial \boldsymbol{A}}{\partial \boldsymbol{Q}} \\ \frac{\partial \boldsymbol{\theta}}{\partial \boldsymbol{I}} & \frac{\partial \boldsymbol{\theta}}{\partial \boldsymbol{Q}} \end{vmatrix} = \begin{vmatrix} \frac{\boldsymbol{I}}{\boldsymbol{A}} & \frac{\boldsymbol{Q}}{\boldsymbol{A}} \\ -\frac{\boldsymbol{Q}}{\boldsymbol{A}^2} & \frac{\boldsymbol{I}}{\boldsymbol{A}^2} \end{vmatrix} = \frac{1}{\boldsymbol{A}}.
$$

The joint PDF becomes independent of $\boldsymbol{\theta}$, and then describes the PDF for the amplitude of the samples

$$
p(\boldsymbol{A}) = \frac{\boldsymbol{A}}{2\pi\sigma^2} e^{-\frac{\boldsymbol{A}^2}{2\sigma^2}}
$$

This PDF is a Rayleigh distribution. The lower panels of figure 3.1 shows that the amplitude of the RD processed noise data before and after cancellation follows this distribution, and the same detection algorithm can therefore be used in both cases.

3.2 Signal to noise ratio

It is useful to define a signal to noise ratio as

$$
SNR_{dB} = 10 log_{10}\left(\frac{|RD[n, m]|^2}{\text{Noise floor estimate}}\right) \tag{3.6}
$$

for the processed data, in order to be able to quantify the effect of signal processing on targets. $|RD[n, m]|$ denotes the amplitude of the component in row n and column m of the RD matrix. As stated in 3.1, the noise of the RD matrix follows a normal distribution with zero mean value. The noise floor estimate is assumed to be the expectancy value of the squared of the amplitude of the noise samples,

$$
\begin{aligned}
E[\boldsymbol{A}^2] &= E[\boldsymbol{I}^2 + \boldsymbol{Q}^2] \\
&= E[\boldsymbol{I}^2] + E[\boldsymbol{Q}^2] \\
&= \sigma^2 + \sigma^2 \\
&= 2\sigma^2
\end{aligned} \tag{3.7}
$$

where I and Q denotes the real and imaginary part of the noise samples respectively. Because the I and Q data of the noise samples are assumed to be uncorrelated, this is the same as two times the variance of either the real or the imaginary part of the samples, where the variance is given in (3.4). The RD processed data in the report are therefore given as
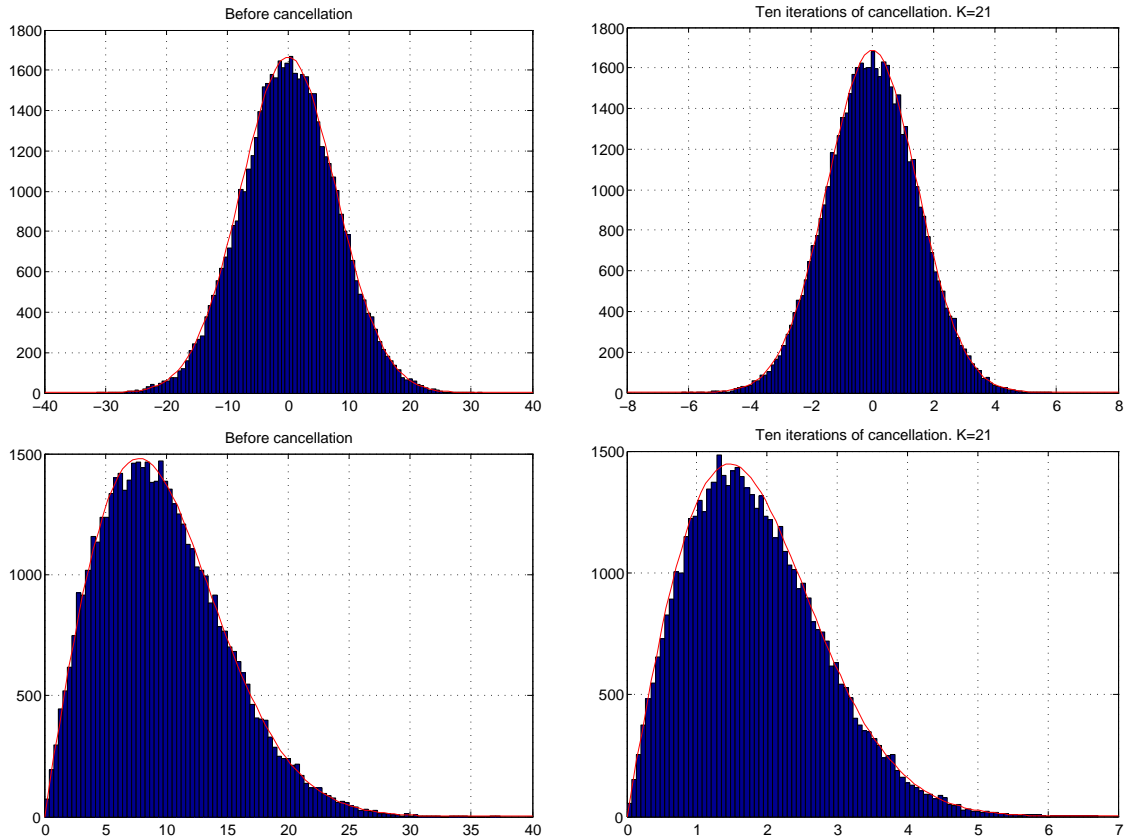
Figure 3.1   Probability distributions for the real part and for the absolute value of 50601 samples assumed to only contain noise. Upper panels: Real part of noise samples, before and after cancellation. Red line shows a Gaussian distribution with the same standard deviation as the noise samples. Lower panels: Amplitude of the noise samples, before and after cancellation. Red line shows a Rayleigh distribution with parameters found from the noise samples considered.

$$SNR_{dB} = 10 log_{10}\Big(\frac{|RD[n,m]|^2}{2\sigma^2}\Big) \tag{3.8}$$

unless other is stated.

4   Direct signal cancellation

As explained earlier in the report, the reception of the direct signal in the surveillance channels causes targets of interest to vanish in the background of noise and clutter. We therefore want to cancel out unwanted interference in the surveillance signal, lowering the noise floor and increasing the signal-to-noise ratio (SNR) in order to improve the detection performance. Because of diffraction and scattering, the surveillance signal may contain several copies of the direct signal with different time delays and from different directions, but all at zero Doppler.

4.1 Extensive Cancellation Algorithm

[1, 2] describes a method called Extensive Cancellation Algorithm, which is going to be the focus of this report. This method assumes a good reference signal obtained by e.g. a separate reference antenna pointing at the transmitter. The method subtracts complex weighted delayed reference signals from the surveillance signal, where the weights have been computed by means of the least mean squares (LMS) method. More precisely, the weights $\boldsymbol{\alpha}$ are obtained by minimizing the norm

$$\min_{\boldsymbol{\alpha}} ||\boldsymbol{s}_{sur} - X\boldsymbol{\alpha}||^2 \tag{4.1}$$

where the matrix X consists of K reference signals ($\boldsymbol{s}_{ref,d_k}$) delayed by d_k samples, corresponding to the ranges at which we want to remove the interference. If one wants to remove the incoming signals in the first five range bins, then d_k and X become

$$d = (0, 1, 2, 3, 4) \tag{4.2}$$

$$X = \begin{bmatrix} \boldsymbol{s}_{ref}[1] & 0 & 0 & 0 & 0 \\ \boldsymbol{s}_{ref}[2] & \boldsymbol{s}_{ref}[1] & 0 & 0 & 0 \\ \boldsymbol{s}_{ref}[3] & \boldsymbol{s}_{ref}[2] & \boldsymbol{s}_{ref}[1] & 0 & 0 \\ \boldsymbol{s}_{ref}[4] & \boldsymbol{s}_{ref}[3] & \boldsymbol{s}_{ref}[2] & \boldsymbol{s}_{ref}[1] & 0 \\ \boldsymbol{s}_{ref}[5] & \boldsymbol{s}_{ref}[4] & \boldsymbol{s}_{ref}[3] & \boldsymbol{s}_{ref}[2] & \boldsymbol{s}_{ref}[1] \\ \vdots & \vdots & \vdots & \vdots & \vdots \\ \boldsymbol{s}_{ref}[T] & \boldsymbol{s}_{ref}[T-1] & \boldsymbol{s}_{ref}[T-2] & \boldsymbol{s}_{ref}[T-3] & \boldsymbol{s}_{ref}[T-4] \end{bmatrix} \tag{4.3}$$

where T is the size of $\boldsymbol{s}_{ref}$ and $\boldsymbol{s}_{sur}$.

The L^2 norm in (4.1) can be written as

$$\min_{\boldsymbol{\alpha}} \left[\frac{1}{2} (\boldsymbol{s}_{sur} - X\boldsymbol{\alpha})^H (\boldsymbol{s}_{sur} - X\boldsymbol{\alpha}) \right] \tag{4.4}$$

where the superscript denotes Hermitian conjugation. The minimization in (4.4) is the same as differentiating with respect to $\boldsymbol{\alpha}$, and then solving with respect to $\boldsymbol{\alpha}$ when the derivative equals 0,

$$
\begin{aligned}
\frac{\partial}{\partial \boldsymbol{\alpha}} \left[||\boldsymbol{s}_{sur} - X\boldsymbol{\alpha}||^2 \right] &= \frac{\partial}{\partial \boldsymbol{\alpha}} \left[\frac{1}{2} (\boldsymbol{s}_{sur} - X\boldsymbol{\alpha})^H (\boldsymbol{s}_{sur} - X\boldsymbol{\alpha}) \right] \\
&= \frac{1}{2} (\boldsymbol{s}_{sur} - X\boldsymbol{\alpha})^H \frac{\partial}{\partial \boldsymbol{\alpha}} \left[\boldsymbol{s}_{sur} - X\boldsymbol{\alpha} \right] \\
&\quad + \frac{1}{2} (\boldsymbol{s}_{sur} - X\boldsymbol{\alpha})^H \frac{\partial}{\partial \boldsymbol{\alpha}} \left[\boldsymbol{s}_{sur} - X\boldsymbol{\alpha} \right] \\
&= (\boldsymbol{s}_{sur} - X\boldsymbol{\alpha})^H X \\
&= 0. \tag{4.5}
\end{aligned}
$$

This gives the following expression for $\boldsymbol{\alpha}$

$$\boldsymbol{\alpha} = (X^H X)^{-1} X^H \boldsymbol{s}_{sur} \tag{4.6}$$

The surveillance signal after cancellation then becomes

$$
\begin{aligned}
\boldsymbol{s}_{DSC} &= \boldsymbol{s}_{sur} - X\boldsymbol{\alpha} \\
&= \boldsymbol{s}_{sur} - \sum_{k=1}^{K} \boldsymbol{s}_{ref,d_k} \boldsymbol{\alpha}[k] \\
&= \left[I_T - X(X^H X)^{-1} X^H \right] \boldsymbol{s}_{sur} \tag{4.7}
\end{aligned}
$$

where K is the length of $\boldsymbol{\alpha}$ and I_T the $T \times T$ unit matrix.

There are many different approaches when deciding on what and how many ranges (with the corresponding delays d_k) to remove the direct signal from. One method could be to cancel out the signal at zero Doppler range bins in the RD matrix with response above a given level. The approach used in this report is to locate the range bin at zero Doppler in the RD matrix with the highest response. This range, along with some range bins at each sides are chosen.

Several iterations of the Extensive Cancellation Algorithm (ECA) may be performed, meaning that the subtraction in (4.7) gets performed several times, chosing new values of d_k and updating $\boldsymbol{\alpha}$ between each iteration/subtraction. $\boldsymbol{s}_{sur}$ then gets replaced by $\boldsymbol{s}_{DSC}$ between each iteration. More iterations removes more direct signal interferences and increase the effect of cancellation on targets.

Figure 4.1 shows the zero Doppler bin before cancellation (blue line), after one iteration of cancellation (red line) and after two iterations of cancellation (green line), when ten range bins at each sides of the range bin with the highest response have been chosen. In the first cancellation, $K = 11$ range bins are chosen for cancellation because the first range bin is the range with the highest response, while in the second cancellation $K = 21$, with the highest response at range bin $d_k = 28$.

The greater K is, the more interference is removed in each iteration of cancellation. The number of iterations of cancellation may be reduced by increasing K. A decision on how many ranges to remove interference from in each iteration of cancellation and how many iterations of cancellation to perform therefore has to be made.

5 Results of DSC

5.1 Measurement setup and processing parameters

The processed data are recorded using two different antenna configurations and two different DVB-T channels. Figure 5.1 shows the two configurations. The reference antenna is directed towards the transmitter for both antenna configurations. Data from the channel with center frequency 722MHz are recorded with antenna configuration A, where the angle between the surveillance antenna main
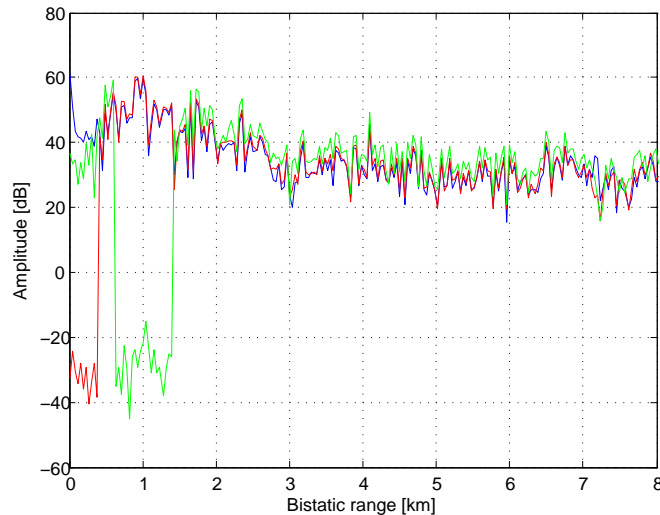
Figure 4.1   Zero Doppler bin from RD matrix. Blue line: Before direct signal cancellation. Red line: One cancellation performed, $d_1 = 1$, $K = 11$ (because signal in the first range bin is to be canceled, only ten bins at higher ranges are to be chosen). Green line: Two cancellations performed, $d_2 = 28$, $K = 21$.

lobe and the transmitter is approximately $90°$. The surveillance antenna is directed towards the main airport of Oslo, which is at a distance of about 25km from the location of the surveillance antenna. The typical airplane approach to the airport then passes between the transmitter and receiving antennas. The surveillance and reference antenna are both Yagi antennas. The transmitting antenna is located at Tryvasshøgda, about 20km from the location of the receiving antennas. The antennas are not in line of sight of the transmitter. For data recorded from the channel of center frequency 546MHz, antenna configuration B is used, where the surveillance antenna is directed towards the transmitting antenna, such that the direct signal is received through the main lobe of the antenna. Dipole antennas are used for both the reference and surveillance antennas in antenna configuration B.
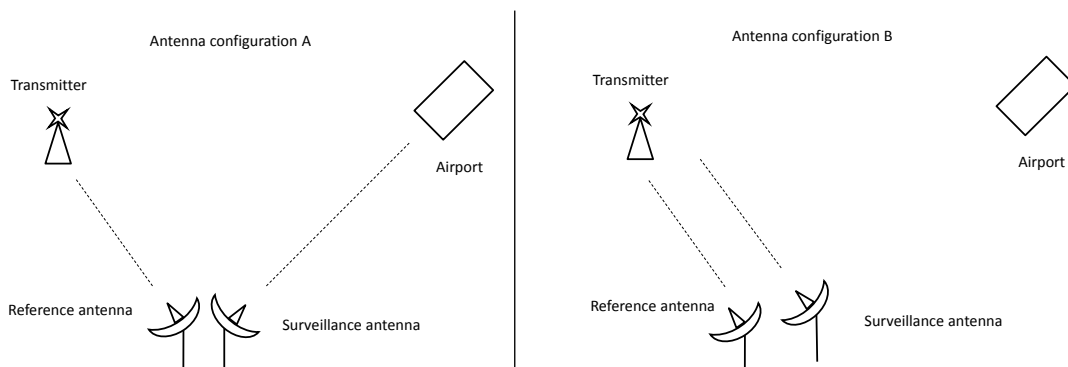

Figure 5.1   Schematic overview of antenna configuration A and antenna configuration B

Targets observed are assumed to mainly be large passenger aircrafts. There have not been used any kind on verification of targets (such as ADS-B), so specific target types are not known.
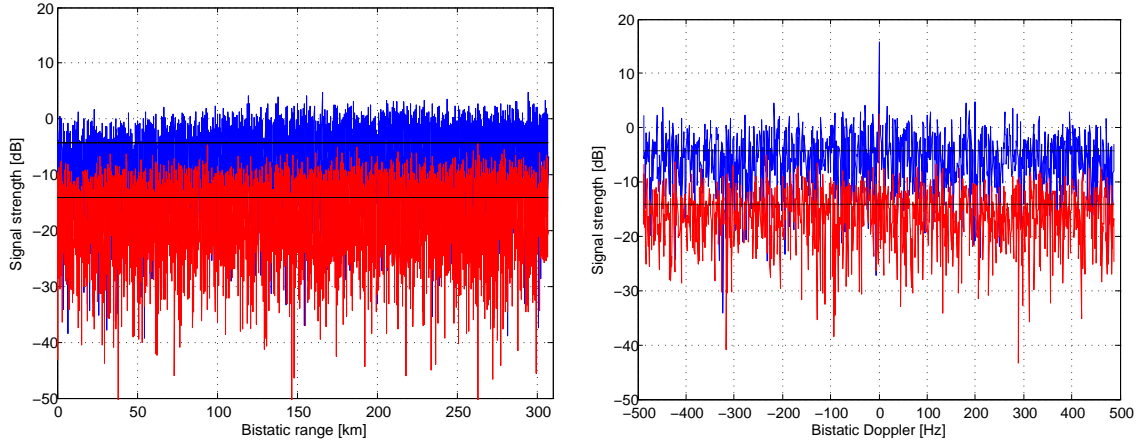
Figure 5.2   Signal strength for RD processed data assumed to only contain noise. Blue line: Before cancellation. Red line: Signal strength after ten iteration of cancellation with $K = 21$ in each iteration. Black lines: Estimated noise level before and after cancellation. Left figure: Signal strength of RD processed data for all ranges and a bistatic Doppler frequency of $150Hz$. Right figure: Signal strength of RD processed data for all Doppler frequencies and bistatic range $230km$.

The RD matrices processed have the dimensions $N = 8192$ samples in range and $M = 1024$ columns in Doppler. With the sampling frequency of $f_s = 8$MHz, this gives each range bin a size of $\Delta r = 37.5$m and a maximum processing range of $r_{max} = 307$km. Each Doppler bin has a size of $\Delta f_D = 0.95$Hz, with the Doppler frequencies in the range $f_D \in [-488.28\text{Hz}, 487.33\text{Hz}]$. The total integration time then become $T_{CPI} = 1.05$s.

Results presented in this report are given as SNR unless other is stated. For some results, the term "signal strength" is used, which denotes the logarithmic values of the amplitude of the correlation and DFT, hence $10 \log_{10} |R[n, m]|^2$, before the data have been divided by the estimated noise floor.

The left panel of figure 5.2 show the signal strength for all ranges and a bistatic Doppler of 150Hz, before cancellation and after ten iteration of cancellation with $K = 21$. The right panel show the signal strength for all Doppler frequencies at a bistatic range of 230km. The data have a slight increase in the average signal strength for long ranges. After cancellation has been performed, the average signal strength is about the same at all ranges. 50601 samples located between $281, 21$km and 300km in range and 350Hz and $445, 4$Hz in Doppler are used to estimate the noise expectancy σ (see section 3.2 for details).

5.2   Results

Figures 5.3 and 5.4 show the effect of cancellation on two targets observed with the different antenna configurations. The lower panels show the results of RD processing for an interval of range and Doppler surrounding the targets. The color scale show the SNR given by (3.8), where 0dB (dark blue) is set as the lower limit and represents the noise floor. The upper limit has been set to 20dB.
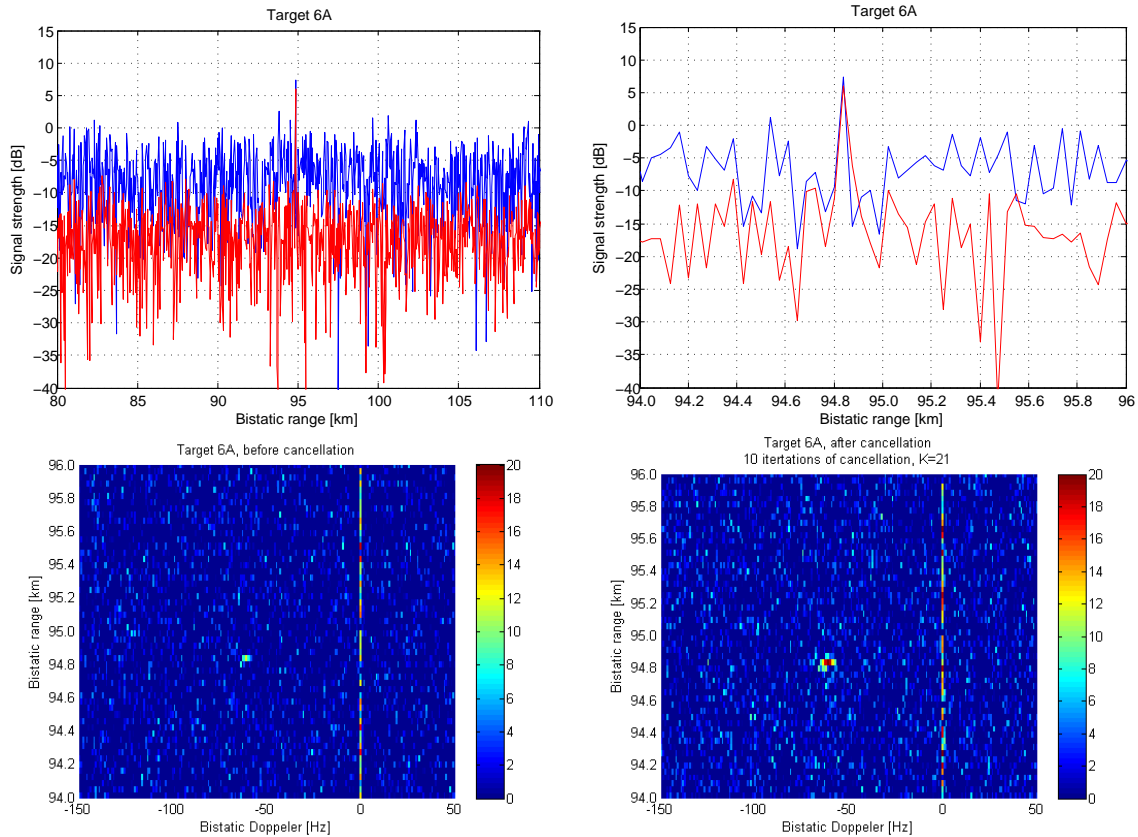
*Figure 5.3   Upper panels: Signal strength in the vicinity of target 6A, at Doppler frequency $-61.0Hz$.
Blue curve: Before cancellation. Red curve: After cancellation.
Lower panels: SNR, given by (3.8), around target 6A before and after cancellation. Ten
iterations of cancellation with $K = 21$. Data are recorded with antenna configuration
A.*

Values below and above these values are either indicated by dark blue or dark red, respectively.

Target 6A had before cancellation a SNR of about 12dB. After ten iterations of cancellations have been performed, the SNR has increased to about 20dB, an increase of about 8dB. The estimated noise floor, $2\sigma^2$ has been reduced by 10dB. This shows that the signal strength of the target has been reduced by about 2dB. Target 6B initially had a SNR of about -5dB, hence below the noise floor. Such a weak target would not be detected by a radar. After cancellation, the target SNR has experienced an increase of about 23dB, which makes the target possible to detect. The noise floor has been reduced by 14dB, which is less than the increase in the target SNR. The signal strength of target 6B has therefore been increased by about 9dB.

Table 5.1 shows the reduction in the estimated noise floor with increasing number of iterations of cancellation, with $K = 21$ in each iteration, for both antenna configurations. The mean noise level for a given antenna configuration does not vary much from one coherent processing interval to the next. The noise floor for data from antenna configuration A decreases about 10dB, while the noise floor in configuration B decreases about 14dB. The table shows that only the first two iterations of
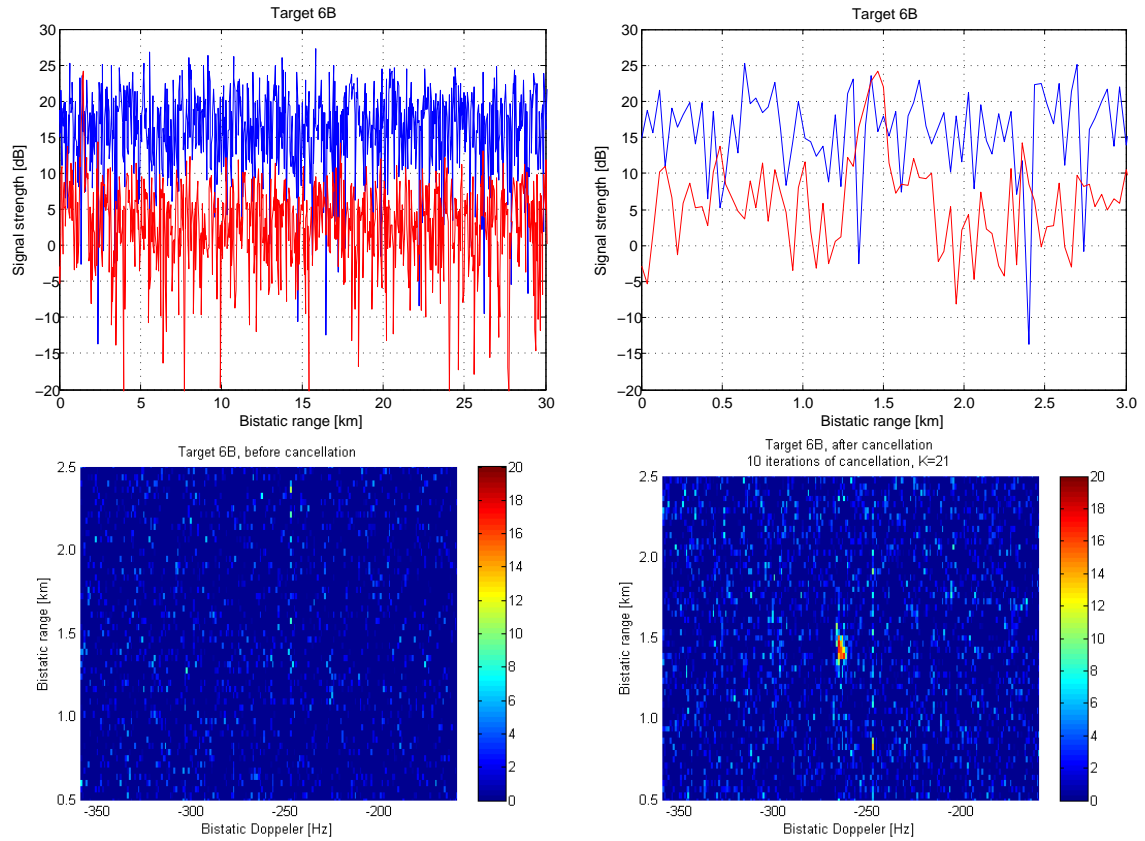
*Figure 5.4   Upper panels: Signal strength in the vicinity of target 6B at Doppler frequency $-266.1Hz$. Blue curve: Before cancellation. Red curve: After cancellation.
Lower panels: SNR, given by (3.8), around target 6B before and after cancellation. Ten iterations of cancellation with $K = 21$. Data are recorded with antenna configuration B.*

cancellation have a significant effect on the noise level. Figure 5.5 shows the behavior of the noise floor for data from antenna configuration A as a function of number of iterations of cancellation.

Table 5.2 shows the increase in SNR for ten targets observed with antenna configuration A and ten targets with configuration B. Targets from the same antenna configuration are all processed with the same integration time T_{CPI}, but are located in different processing intervals. Targets from antenna configuration A have experienced an average increase of 10dB, ranging from 8dB to 12dB. The average increase for targets observed with antenna configuration B is 20dB, ranging from 13dB to 30dB. Some targets from this configuration have a signal strength less than the estimated noise floor before cancellation, while the signal strength has increased to a level possible to detect after cancellation has been performed.

Figure 5.6 shows the average increase in SNR of target 1B, 2B and 3B for $K = 1, 3, 5, 7, 9, 11, 13, 15, 17, 19$ and 21, and for 1 to 15 iterations of cancellations. As K is increased, there is less to gain by increasing K further, given that the ranges are chosen as explained in section 4. We note that there is little to gain by increasing K beyond 10 or so.
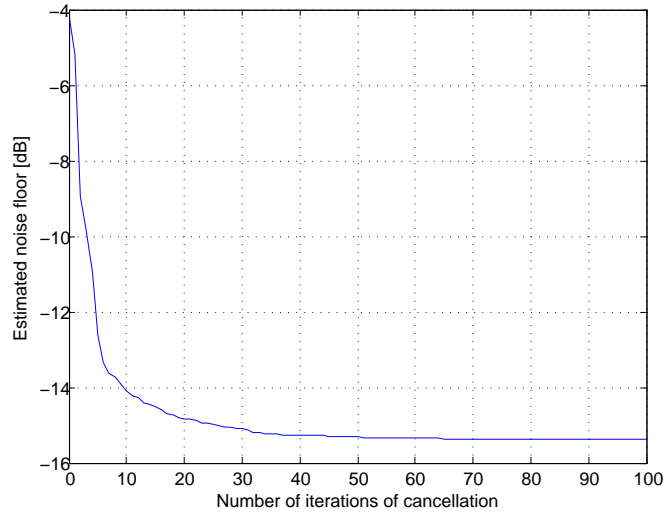
Figure 5.5　*Estimated noise floor ($10\log_{10}(2\sigma^2)$) as a function of the number of iterations cancellation performed. Data from antenna configuration A.*

Number of iterations	Antenna config. A	Antenna config. B
Before DSC	-4.2 dB	20.8 dB
After 1st	-5.2 dB	10.8 dB
After 2nd	-9.0 dB	8.7 dB
After 3rd	-9.8 dB	7.6 dB
After 4th	-10.9 dB	7.3 dB
After 5th	-12.6 dB	7.2 dB
After 6th	-13.3 dB	7.1 dB
After 7th	-13.6 dB	7.0 dB
After 8th	-13.8 dB	6.8 dB
After 9th	-13.9 dB	6.7 dB
After 10th	-14.1 dB	6.5 dB
Total decrease	**9.9 dB**	**14.3 dB**

Table 5.1　*Reduction in the estimated noise floor, $2\sigma^2$ for antenna configurations A and B, when ten iterations of cancellation are performed. $K = 21$ ranges for cancellation have been selected in each iteration.*

Antenna configuration A				
	(Range, Doppler) Bistatic	**SNR before DSC**	**SNR after DSC**	**Increase in SNR**
Target 1A	(16.1 km, -376.7 Hz)	19 dB	28 dB	9 dB
Target 2A	(0.7 km, -140.2 Hz)	12 dB	24 dB	12 dB
Target 3A	**(60.5 km, -24.8 Hz)**	**9 dB**	**17 dB**	**8 dB**
Target 4A	**(15.6 km, -371.0 Hz)**	**17 dB**	**27 dB**	**10 dB**
Target 5A	**(0.9 km, -184.1 Hz)**	**13 dB**	**25 dB**	**12 dB**
Target 6A	**(94.8 km, -61.0 Hz)**	**12 dB**	**20 dB**	**8 dB**
Target 7A	(3.6 km, -330.9 Hz)	19 dB	29 dB	10 dB
Target 8A	(19.3 km, -349.0 Hz)	3 dB	13 dB	10 dB
Target 9A	(11.7 km, -96.3 Hz)	14 dB	25 dB	11 dB
Target 10A	**(11.9 km, -332.8 Hz)**	**16 dB**	**26 dB**	**10 dB**
Average increase				**10 dB**
Antenna configuration B				
	(Range, Doppler) Bistatic	**SNR before DSC**	**SNR after DSC**	**Increase in SNR**
Target 1B	(1.4 km, -156.4 Hz)	21 dB	39 dB	18 dB
Target 2B	(11.9 km, 49.6 Hz)	13 dB	30 dB	17 dB
Target 3B	(1.1 km, -24.8 Hz)	15 dB	34 dB	19 dB
Target 4B	**(1.5 km, -151.6 Hz)**	**9 dB**	**28 dB**	**19 dB**
Target 5B	**(13.6 km, 51.5 Hz)**	**0 dB**	**14 dB**	**14 dB**
Target 6B	(1.5 km, -266.1 Hz)	-5 dB	18 dB	23 dB
Target 7B	(3.4 km, -186.0 Hz)	-8 dB	17 dB	25 dB
Target 8B	(1.8 km, 171.7 Hz)	-12 dB	18 dB	30 dB
Target 9B	**(7.2 km, -238.4 Hz)**	**-6 dB**	**18 dB**	**24 dB**
Target 10B	**(13.8 km, -51.5 Hz)**	**-2 dB**	**11 dB**	**13 dB**
Average increase				**20 dB**

Table 5.2   Target SNR, before cancellation and after ten iterations of cancellation with $K = 21$ have been performed. Integration time of $T_{CPI} = 1.05s$. The alternating bold and normal format of the text indicate targets that are located in different $1.05s$ time intervals. Upper table: Antenna configuration A. Lower table: Antenna configuration B.
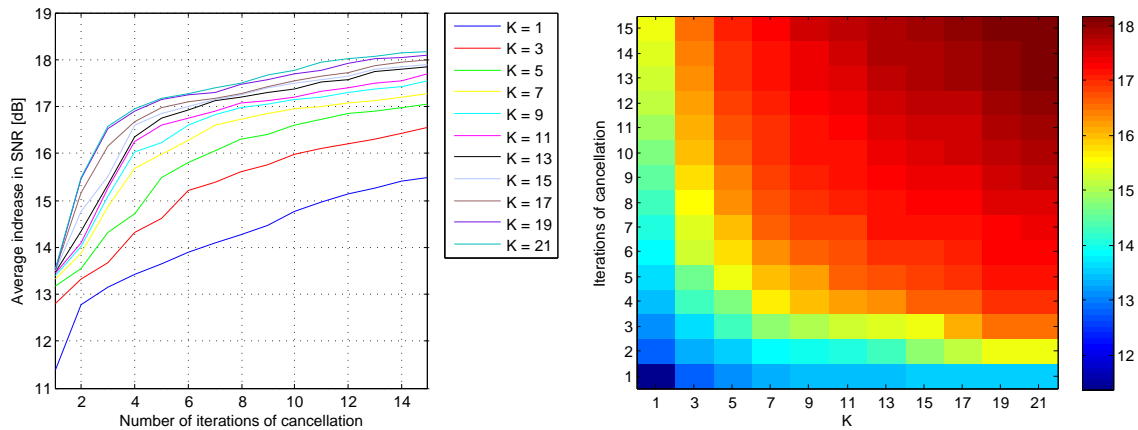
Figure 5.6   *Average increase in SNR (no cancellation equals zero increase) of targets 1B, 2B and 3B as a function of K and number of iterations of cancellation. Left panel: Average increase in SNR as a function of number of iterations of cancellation. Each line represents one K, ranging from $K = 1$ to $K = 21$ with a step of 2. Right panel: The color bar shows the average increase in SNR, presented in dB.*

6   Conclusion

Passive radars may encounter problems with a strong direct signal from the transmitter interfering in the surveillance antenna of the radar. The direct signal increases the noise, which can mask the response of targets. In this report, a method for removing the direct signal by means of digital signal processing has been used. The Extensive Cancellation Algorithm, which is based on the least mean squares method [1, 2], computes complex weights such that weighted copies of the reference signal, with different time delays can be subtracted from the surveillance signal. A good reference signal must have been obtained by other means (e.g. by a separate antenna pointing at the transmitter).

In order to quantify the effect of direct signal cancellation on targets, a signal to noise ratio based on an estimated noise floor is established. The noise before cancellation has a slight increase at long ranges. The noise floor is estimated from the RD matrix far out in range and Doppler where there are assumed to be no targets. The estimated noise floor therefore may be higher than the actual noise floor around targets at closer ranges. The consequence of this on the effect of direct signal cancellation are not studied further in this report, but figure 5.2 indicates that the effect is at most s few dB.

Cancellation clearly has an effect on the target SNR, ten targets from antenna configuration A and configuration B experience an average increase of about 10dB and 20dB, respectively. Some targets observed with antenna configuration B had initially a signal level below the noise floor (negative SNR). After cancellation, the strength of the targets has increased to a level above the noise floor, enabling detection. Because the surveillance antenna in configuration B is pointing almost directly towards the transmitter, the main lobe of the surveillance antenna receives the direct signal. The direct signal is therefore a more dominant part of the surveillance signal from configuration B, and

the DSC seems to have a greater effect both on the target SNR and the reduction in noise floor.

The first iterations of cancellation have the largest effect on the reduction in the noise floor. If 100 iterations of cancellations with $K = 21$ are performed, the noise floor does not experience any significant further decrease compared to only ten iterations with $K = 21$.

More iterations of cancellation and large values of K removes more interference. As figure 5.6 show, the increase in SNR settles at a level of about 18dB when the number of iterations approach 15 and K becomes above 10 or so. The substantial number of iterations or the large value of K required to achieve most of the SNR increase, indicate that many sources of ground clutter contribute to the direct signal interference.

Direct signal cancellation by means of the LMS method clearly has an effect on the target SNR, such that even targets having initially a SNR lower than the average noise level may be detected after cancellation.

The method for cancellation introduced in this report may not only be restricted to the direct signal of zero Doppler frequency interfering in the surveillance antenna [3]. Assume there is a strong target present at a none zero Doppler frequency, which may mask other weaker targets. By adding the desired frequency shifts to the reference signals in matrix X in (4.3), the signal component at the Doppler frequency and range can be removed [3].

Appendix A Abbreviations

FFI	Norwegian Defence Reasearch Establishment
DSC	Direct Signal Cancellation
DVB-T	Digital Video Broadcasting — Terrestrial
SNR	Signal to Noise Ratio
RD	Range-Doppler
LMS	Least Mean Squares
DFT	Discrete Fourier Transform
FFT	Fast Fourier Transform
CPI	Coherent Processing Interval
Hz	Hertz (cycles per second)
MHz	Megahertz
I/Q	In-phase and Quadrature-phase
PDF	Probability distribution function
s	Seconds
dB	Decibels

Appendix B   Symbols

Symbol	Definition
$\boldsymbol{x}$	Vector notation
$\boldsymbol{x}[n]$	n'th component of vector x
$\boldsymbol{x}^*$	Complex conjugate of each component in vector x
$\mathcal{F}(\boldsymbol{x})$	Fourier transform of vector x
X	Matrix notation
X^H	Conjugate transpose of the matrix X
$\mathcal{F}(X)$	Fourier transform of matrix X
$\mathcal{F}^{-1}(X)$	Inverse Fourier transform of matrix X
f_s	Sampling rate
f_D	Doppler frequencies
$\boldsymbol{s}_{ref}$	Reference signal
$\boldsymbol{s}_{sur}$	Surveillance signal
N	Range-Doppler matrix dimension in range
M	Range-Doppler matrix dimension in Doppler
S_{ref}	Reference matrix
S_{sur}	Surveillance matrix
$c[n, f_D]$	Correlation between reference and surveillance signal with Doppler shifts
R	Correlation between reference and surveillance matrix
RD	Range-Doppler matrix
T_{CPI}	Integration time / coherent processing interval
I	In phase demodulated data
Q	Quadrature demodulated data
j	Square root of -1
$E[\boldsymbol{x}]$	Expectancy value of vector x
σ	Standard deviation

References

[1] R. Cardinali, F. Colone, C. Ferretti, and P. Lumbardo. Comparison of clutter and multipath cancellation techniques for passive radar. *IEEE Radar Conference 2007*, pages 469–474, April 2007.

[2] W.L. Melvin and J.A. Scheer. *Principles of Modern Radar, Advanced Techniques*, volume 2, chapter 17.3. SciTech Publishing, 2013.

[3] F. Colone and P. Lombardo R. Cardinali. Cancellation of clutter and multipath in passive radar using a sequential approach. *IEEE Radar Conference*, 2006.

[4] Norsk Televisjon. http://www.ntv.no/, 2014.

[5] R.G. Lyons. *Understanding Digital Signal Processing*, chapter 2. Prentice Hall, 2004.

[6] J. M. Christiansen. Dvb-t based passive bistatic radar. Technical report, Norwegian Defence Research Establishment, 2010.

[7] M. Cherniakov. *Bistatic Radar, emerging technology*, pages 295–303. John Wiley and Sons Ltd, 2008.

[8] B. W. Jarvis E. C. Ifeachor. *Digital Signal Processing, A practical approach*, chapter 2 and 4. Addison-Wesley Publishing Company, 1993.

[9] N. Levanon. *Radar Principles*, pages 39–44. Wiley-Interscience publication, 1988.

[10] S. O. Rice. *Mathematical Analysis of random noise*. Bell Thelephone Labs Inc New York, 1952.